Geophysical Research Letters®

Toward a Better Understanding of Wildfire Behavior in the Wildland-Urban Interface: A Case Study of the 2021 Marshall Fire

Timothy W. Juliano[1] ⓘ, Neil Lareau[2] ⓘ, Maria E. Frediani[1], Kasra Shamsaei[2] ⓘ, Masih Eghdami[1] ⓘ, Karen Kosiba[3], Joshua Wurman[3], Amy DeCastro[1], Branko Kosović[1], and Hamed Ebrahimian[2] ⓘ

[1]Research Applications Laboratory, National Center for Atmospheric Research, Boulder, CO, USA, [2]University of Nevada, Reno, NV, USA, [3]University of Illinois at Urbana–Champaign, Champaign, IL, USA

Abstract On 30 December 2021, the Marshall Fire devastated the Boulder, Colorado region. The fire initiated in fine fuels in open space just southeast of Boulder and spread rapidly due to the strong, downslope winds that penetrated into the Boulder Foothills. Despite the increasing occurrence of wildland-urban interface (WUI) disasters, many questions remain about how fires progress through vegetation and the built environment. To help answer these questions for the Marshall Fire, we use a coupled fire-atmosphere model and Doppler on Wheels (DOW) observations to study the fire's progression as well as examine the physical drivers of its spread. Evaluation of the model using the DOW suggests that the model is able to capture general characteristics of the flow field; however, it does not produce as robust of a hydraulic jump as the one observed. Our results highlight limitations of the model that should be addressed for successful WUI simulations.

Plain Language Summary Wildland-urban interface (WUI) fires are increasing in the United States and around the world as the built environment continues to expand into the wildland. To better inform real-time management of active wildfires, it is critical that the scientific community can better predict WUI fire spread. In this study, we rely on multiple observational platforms, including the "Doppler on Wheels" radar, to investigate the performance of a state-of-the-art fire behavior model that links with a weather model during the Marshall Fire, which was a recent WUI fire that occurred in Colorado. While the modeling system performs well during the fire's initial propagation in fine fuels, it is unable to accurately predict spread in the built environment. While turbulence-resolving simulations can accurately represent atmospheric flow features, more reliable predictability of wildfire behavior in the WUI will require consideration of urban fuels and fire ember spotting.

1. Introduction

Wildfire activity in the United States (U.S.) and across the globe has increased markedly over the last several decades (e.g., Balch et al., 2017; Dennison et al., 2014; Iglesias et al., 2022; Westerling et al., 2006). In the U.S., many of the recent wildfire seasons have involved long and intense burning periods, leading to the loss of life and property, as well as poor air quality (e.g., Buchholz et al., 2022) and reductions in solar energy production as a result of smoke generation (e.g., T. W. Juliano, Jiménez, et al., 2022). Global climate models suggest that the recent trend of more large-scale fire events will continue and even increase in the future (e.g., Abatzoglou & Williams, 2016; Yoon et al., 2015; Yue et al., 2013). As part of the complexity, the so-called wildland-urban interface (WUI) is rapidly growing (e.g., Burke et al., 2021; Radeloff et al., 2018) and, therefore, amplifying the direct threat of wildfires on daily human activities.

Several notable WUI fires have occurred over the past decade in the U.S., primarily in California, including the Tubbs Fire (2017; e.g., Coen et al., 2018; Mass & Ovens, 2019), Camp Fire (2018; e.g., Brewer & Clements, 2019; Mass & Ovens, 2021), Woolsey Fire (2018; e.g., Keeley & Syphard, 2019), and Thomas Fire (2017; e.g., Fovell & Gallagher, 2018). One commonality between these wildfires is that they were considered wind-driven fires, allowing them to expand rapidly and devastate nearby communities in their paths. In California, so-called "Santa Ana" (e.g., Raphael, 2003, and references therein) or "Diablo" (e.g., Liu et al., 2021) wind events are often associated with destructive wind-driven wildfires (e.g., Nauslar et al., 2018; Smith et al., 2018). Wind-driven WUI fires are also a concern in regions outside of the U.S., including Australia (e.g., Cruz et al., 2012), France (e.g., Ganteaume, 2020), and Greece (e.g., Efthimiou et al., 2020).

The Marshall Fire is an example of a catastrophic wind-driven, WUI fire event that occurred just outside of Boulder, Colorado, U.S. on 30 December 2021 (Fovell et al., 2022), causing two deaths and destroying more than 1,000 buildings, leading to over $500 M in damages. The fire ignited near the Marshall Mesa in the presence of strong winds that exceeded 40 m s^{-1}, and it began spreading rapidly in dry, fine fuels driven by intense, westerly winds. Approximately 1 hr after ignition, the fire transitioned into an urban conflagration, including "hopping" the six-lane Highway-36 via ember spotting. The large-scale meteorological setup favored a downslope wind-storm along the Front Range (Fovell et al., 2022), which is a relatively common occurrence in this geographical region during the cold season (e.g., Durran, 1990; Whiteman & Whiteman, 1974).

In this study, we use observations and numerical simulations to examine the impact of the meso- and micro-scale meteorology on the Marshall Fire behavior. Specifically, we use a state-of-the-art numerical framework, the Weather Research and Forecasting (WRF) model coupled with a fire behavior model (WRF-Fire), as well as measurements from the Doppler on Wheels (DOW) radar system, to address the following fundamental questions related to the topic of wildfire-weather: (a) *What were the observed and modeled atmospheric flow characteristics during the Marshall Fire? And (b) How well does the WRF-Fire model reproduce the Marshall Fire spread in the WUI?*

2. Data and Methods

2.1. WRF-Fire Model

The WRF model is a widely used numerical weather prediction system (Skamarock et al., 2019) proven to be a powerful tool for simulating the full range of atmospheric scales, including meso- and micro-scales (e.g., Mazzaro et al., 2017; Muñoz-Esparza et al., 2017; Rai et al., 2019). Here, we utilize WRF in a one-way nested, mesoscale to microscale configuration (e.g., Haupt et al., 2019) whereby the inner domain is turbulence-resolving. The WRF domains are positioned to capture the westerly inflow that plays an important role on the wildfire prop-agation (Figure S1 in Supporting Information S1). To examine the Marshall Fire evolution, we conduct WRF simulations with a fire behavior model based on the Coupled Atmosphere-Wildland Fire Environment (Clark et al., 2004; Coen, 2013). This coupled fire-weather model is called WRF-Fire (Coen et al., 2013). Our model setup and physics options closely follow those used in recent studies by our team of the East Troublesome Fire (DeCastro et al., 2022) and the Camp Fire (Shamsaei et al., 2023), and additional details may be found in Text S1 in Supporting Information S1.

2.2. DOW Measurements

The DOW platform was deployed during the Marshall Fire to capture the three-dimensional smoke/ash plume and flow structures. Operating at 3-cm wavelength, the DOW is a mobile/quick deployable Doppler radar with high spatial resolution (50 m gate length and 160 m × 160 m beam size at 10 km range), allowing it to measure microscale structures (Wurman et al., 1997, 2021). During this deployment, the DOW operated mostly in a rastered Plan Position Indicator scanning mode, with elevation scans ranging from ∼0.5–23° (adjusted through-out the deployment) above the horizon. Parameters derived from the DOW observations and relevant to this study include reflectivity, radial velocity, and spectrum width. More information about these parameters is provided in Text S2 in Supporting Information S1.

3. Fire Spread in the WUI

The Marshall Fire had two reported initial ignition points, occurring at 18:08 and 19:00 UTC and approximately several 100 s of meters apart (see Text S3 in Supporting Information S1 for more information). Thus, in our WRF-Fire simulations, we first ignite two separate fires. Both ignition points were in dry, short grass fuels. During the early stages of the fire, the combination of fuels and strong (∼25 m s^{-1}), westerly winds supported rapid fire growth in the Marshall Mesa area (magenta star in Figure 1). At 19:00 UTC, the initial burn region in the model takes on a finger-like structure, with spotting on the east and southern flanks as it approaches Highway 36 (Figure 1).

According to Visible Infrared Imaging Radiometer Suite (VIIRS) fire detections at 19:25 UTC, the fire had spot-ted across Highway-36 to cause secondary ignitions (Figure S3 in Supporting Information S1), but the simulated fire does not cross the highway via spotting until 19:45 UTC (cf. Figure 1), at which time another burning lobe to
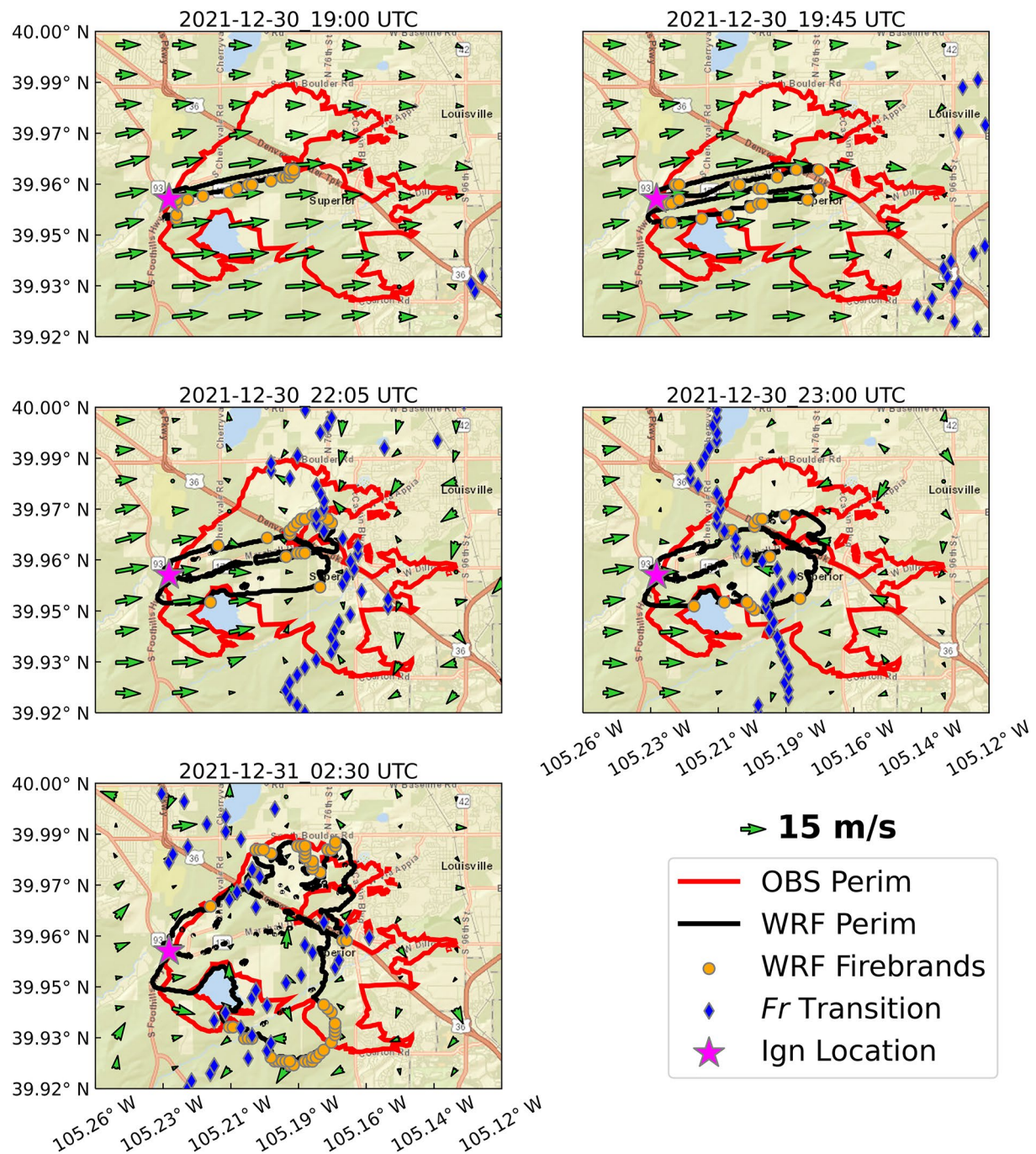
Figure 1. Temporal progression of the Marshall Fire spread. The magenta star represents the approximate location of the initial fire ignitions, the red line represents the final observed perimeter, and the black line represents the WRF-Fire perimeter at the indicated time. The orange circles represent firebrand landing locations according to WRF-Fire. Flow transitions from supercritical to subcritical are shown by the blue diamonds. Also shown are 10 m wind arrows according to the key.

the south originating from the second ignition has nearly reached the highway. Two snapshots from VIIRS shortly after, at 20:15 UTC and 21:00 UTC (Figure S3 in Supporting Information S1), show that the modeled leading edge is too slow and the north-south expansion is too narrow. During this ~1.5 hr period, the intense westerly winds continue across much the region; however, the model shows weaker westerlies and even "reversed" flow intruding (further discussed in Section 4).

By mid-afternoon (22:05 UTC), the rapid fire spread is halted in the model (Figure 1) as it reaches the urban region, where non-burnable fuels are present in the model fuel layer (Figure S2 in Supporting Information S1).
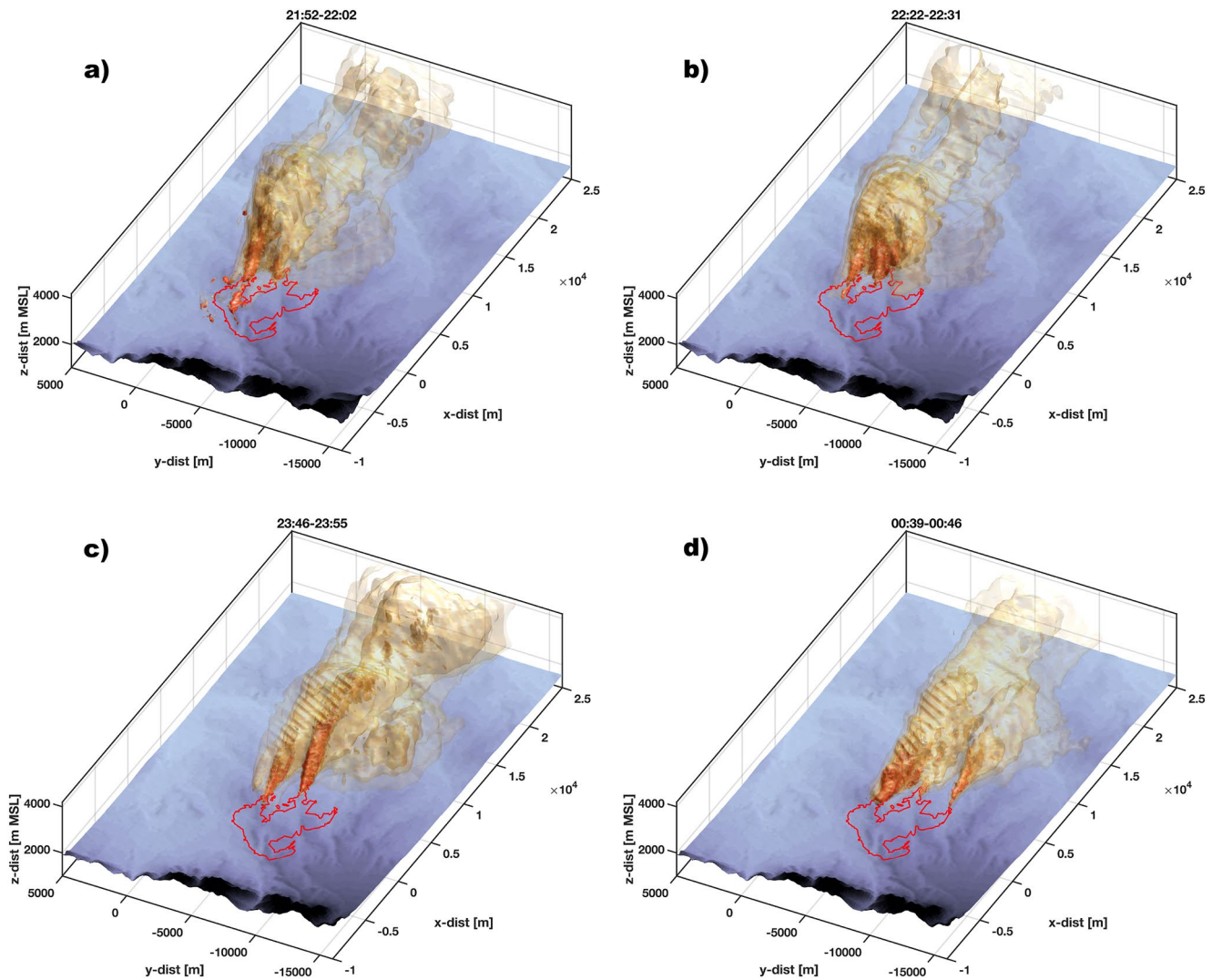
Figure 2. Radar reflectivity isosurfaces showing plume evolution. Transparent Isosurfaces are rendered at −10, 10, 15, 20, 23, 26, and 27 dbZ with colors becoming increasingly red for higher values. The data window (UTC), is shown at the top of each panel. Also shown are the IR fire perimeter (red contour) and terrain elevation (gray shaded relief).

The westerly, low-level flow is confined to the western potion of the area, with winds near the fire front opposing the original fire spread direction. This flow transition will be discussed further in Section 5. Nonetheless, around this time, the DOW reflectivity isosurfaces show active plume cores in two of the main fingers further north and east (Figure 2a), confirming that the model is unable to capture the rapid propagation across Highway-36.

Between 22:05 and 23:00 UTC, the model shows generally slower fire spread compared to previous hours, as it expands the burned region mostly to the north and south due to the relatively weak, variable winds (Figure 1). During this time, and over the next couple of hours, the radar reflectivity isosurfaces indicate that the fire becomes increasingly active in the middle finger (Figures 2b and 2c) before dissipating, while a new southern finger becomes more active (Figure 2d). Only by the evening (02:30 UTC) does the simulated burn area finally spread into Louisville on the north side of Highway-36 and toward the southernmost observed finger (Figure 1). In Section 6, we will discuss potential sources of error in the WRF-Fire simulations.

4. Horizontally Heterogeneous Wind Field

The synoptic-scale and mesoscale meteorology during the Marshall Fire event fostered intense downslope winds along the Front Range (Fovell et al., 2022). A north-south band of strong, westerly flow (gusts >30 m s^{-1}) was
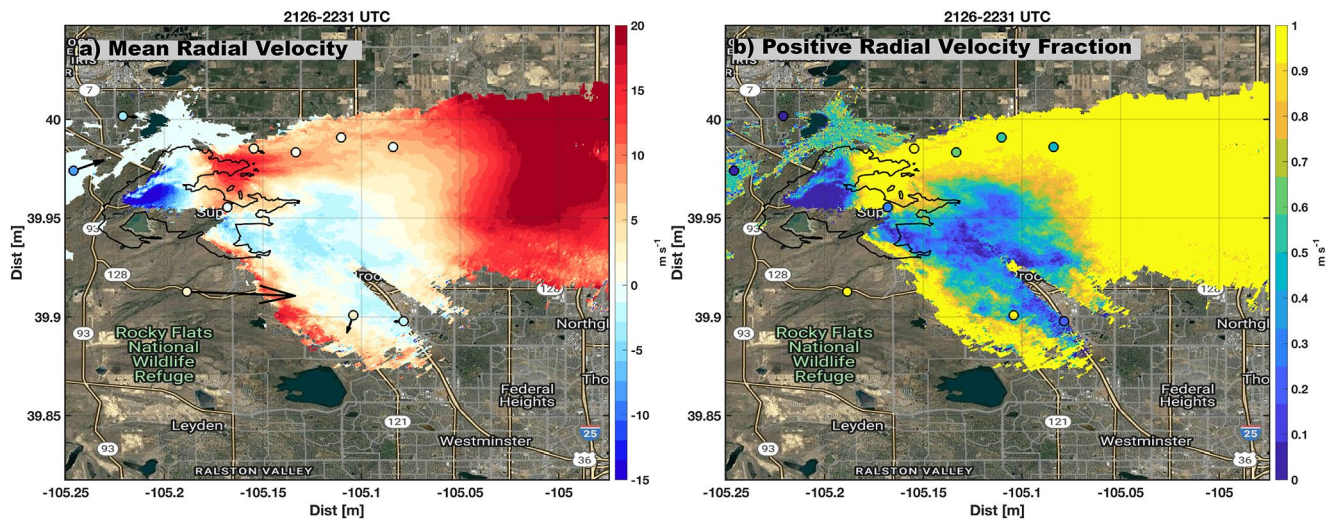
Figure 3. (a) Time-mean radial velocity data with station observations showing mean wind vectors and mean radial velocity (color shaded). (b) Fraction of the time with a positive radial wind component. Both figures also show the final observed perimeter (solid black contour).

positioned along the Boulder Foothills, where the plunging, downslope flow remained attached at the surface, including in the vicinity of the Marshall Fire ignitions. In contrast, many locations not too far to the east generally experienced weaker winds (gusts <20 m s^{-1}) where the flow detached from the surface, as shown in Figure 1 and in agreement with Fovell et al. (2022, their Figure 1). To evaluate the WRF-Fire model's ability to represent the spatially variable, low-level flow during the event, in Figure S4 in Supporting Information S1 we compare observed and modeled time series of the surface stations shown in Figure S1 in Supporting Information S1 and described in Text S4 in Supporting Information S1. By and large, the model performs better at the western stations, where strong, westerly winds persisted before the flow transitioned. Even still, WRF tends to underestimate the strongest observed wind gusts of 40–50 m s^{-1} at CO1 and BLD. This result supports the aforementioned underestimation in model fire spread. Compared to the western area, both observations and WRF show much more variable wind speeds and directions east of the fire. Simulations of a downslope wind storm in the Wasatch Range showed similar spatial variability in the mesoscale flow (Lawson & Horel, 2015).

The horizontal structure and variability in the wind field is captured by the DOW radial velocity observations. Figure 3a shows the time-mean radial velocity for scans below 5°, revealing (a) the strong west-southwest winds across the fire, (b) a region of reversed flow, especially over the southern portions of the fire area, and (c) a subsequent return to west winds aloft and to the east. In Figure 3b, we also show the fraction of the time the radial wind is positive. These data show that within the time-mean reversed flow regions, many locations experience positive winds ∼50% of the time, suggesting that the winds were highly variable. As we will discuss in the next section, the flow variability is related to the presence of a hydraulic jump. Shown in both plots are also station observations (colored circles) that indicate the radial wind component and the vector wind during the averaging period (Figure 3a), as well as the fraction of time with positive winds at each site (Figure 3b). Overall, we find reasonable agreement between the radar and near-surface observations; however, some differences are expected because the height of the radar retrieval volume increases as the radial distance increases according to the DOW scan angle (not shown).

5. Vertical Structure and Flow Evolution

Based on quasi-idealized simulations, Fovell et al. (2022) suggest that a "hydraulic jump-like feature" was present downwind of the strongest winds in the Boulder Foothills. To further explore this aspect of the atmospheric flow, we use model output and DOW observations. In Figure 4, we present east-west vertical cross-sections of the zonal wind component. Each panel represents a different snapshot in time, with the times corresponding to those shown in Figure 1. Throughout the event, the low-level, downslope winds upstream of the fire (west of ∼105.3°W) are consistently strong and capped by a strong inversion where winds diminish quickly with height. This band of intense winds continues eastward, bringing strong westerlies into the Boulder Foothills during the early stages of
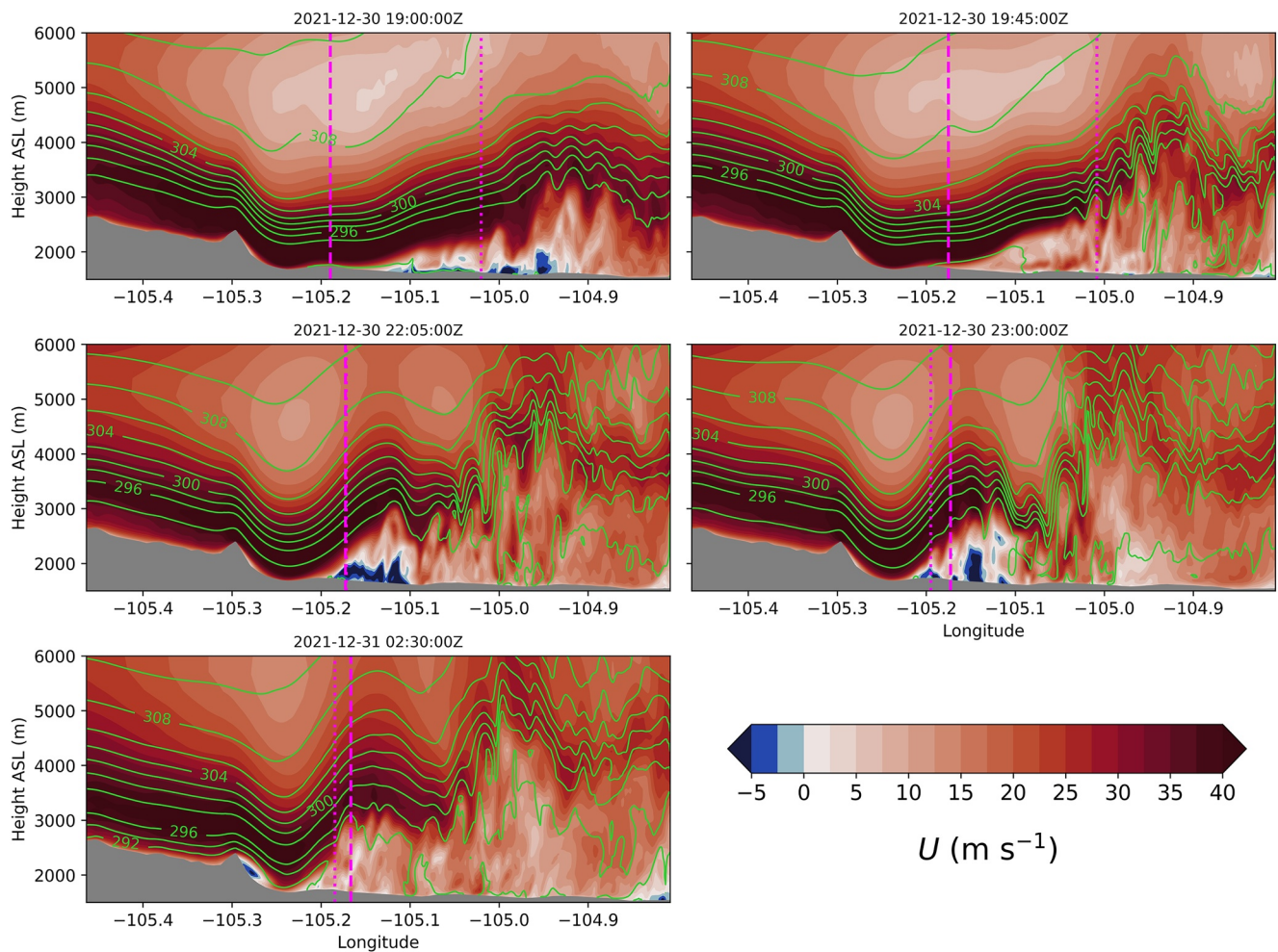
Figure 4. East-west vertical transects (latitude of 40.04°N) showing the *U*-component of the wind speed according to the colorbar, along with isentropes (potential temperature contours) every 2 K in green. The dashed magenta line represents the furthest eastward progression of the fire front in the whole domain. Also plotted is the location of the flow transition (*Fr* = 1; dotted magenta line). Gray shading represents the terrain profile. Times shown are the same as in Figure 1.

the Marshall Fire, and rising with height toward the east (Figure 4). As a result, the atmospheric flow supports the fire's rapid advancement around 1900 UTC (cf. Figure 1). Over the ensuing hours, the wind maximum retreats westward, and, eventually, the vertical structure, which is well-defined by strong thermal stratification and weak vertical motion, breaks down into a more chaotic structure to the east (Figure 4). The strong inversion erodes where the intense winds diminish, as the wavy isentropes (solid green lines) suggest strong vertical mixing within the lower-levels. In the transition zone, a hydraulic jump is evident with a sharp decrease, and even complete reversal, in the zonal winds and vertical displacement of the isentropes. Characteristics of the hydraulic jump are found to be insensitive to the fire's feedback on the atmosphere due to the strong mesoscale forcing (Text S5, Figures S6–S8 and S10 in Supporting Information S1).

The transition from strong flow in a shallow boundary layer to weaker winds as the boundary layer deepens further downwind, with turbulence production in between, are classical characteristics of a hydraulic jump (e.g., Ball, 1956; T. W. Juliano et al., 2017). To probe the dynamical support for the presence of a hydraulic jump, we conduct a Froude Number (*Fr*) analysis along the vertical cross-sections shown in Figure 4. Results presented in Figure S5 in Supporting Information S1 indicate a transition from supercritical (*Fr* > 1) to subcritical flow (*Fr* < 1)—a well-known requirement for the presence of a hydraulic jump. Upstream *Fr* values between 2 and 4 (Figure S5 and Text S6 in Supporting Information S1) suggest a hydraulic jump with a roller (e.g., Chanson, 2009), whereby much of the mean kinetic energy is converted into turbulent kinetic energy (TKE). In this particular case, the WRF model simulates an extraordinary transition, with maximum TKE values exceeding 200 m² s⁻² due to the strong decay in intense westerly winds (Figure S9 in Supporting Information S1).
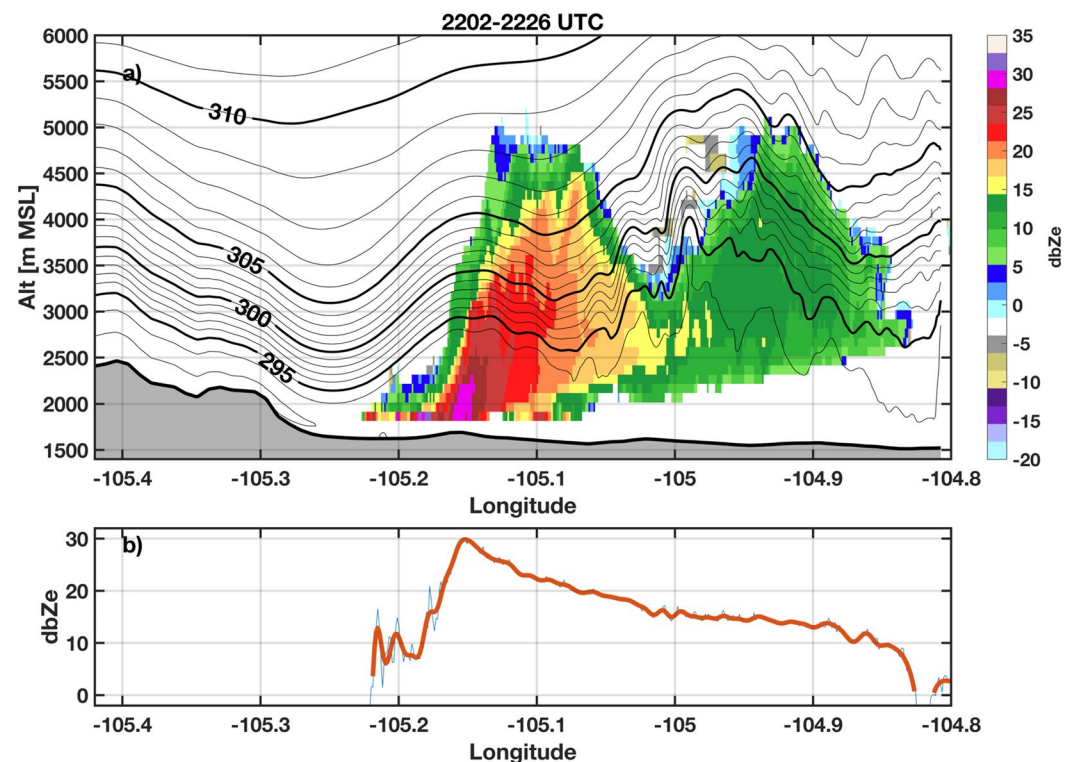
Figure 5. (a) Time and meridional maximum radar reflectivity cross section for the 2202–2226 UTC interval. Reflectivity values are shaded, with potential temperature contours from the Weather Research and Forecasting model (contours every 1 K, bold and labeled every 5 K). Gray shading represents the terrain profile. (b) Column maximum radar reflectivity as a function of longitude.

The hydraulic jump and subsequent gravity wave structures in Figure 4 are readily apparent in a cross section of the radar reflectivity spanning 2202–2226 UTC (Figure 5). Specifically, the DOW data show a leading wave linked to the fire's updraft that is embedded in the hydraulic jump region followed by a subsidence region (i.e., diminishing plume heights) and a second wave crest (Figure 5a). Spectrum width measurements (Figure S11 in Supporting Information S1) show maximum values in the primary plume with a secondary maximum in the downstream wave (qualitatively similar to the TKE field from WRF; cf. Figure S9 in Supporting Information S1). The contemporaneous isentropes extracted from WRF, with the strong thermal inversion acting as a lid for the vertical extent of the modeled smoke plume (Figure S12 in Supporting Information S1), suggest that the simulation underestimates the injection height of smoke and ash in the leading wave. This discrepancy may be due to differences in fire spread rates or a lack of urban fuels in the model: the combustion of urban fuels, which have high fuel loads (e.g., O(100 kg m^{-2}); Bush et al., 1991) relative to the upwind grasses O(0.1–1 kg m^{-2}), may have produced more intense heat release in reality compared to what was simulated. Nonetheless, the structure of the second wave agrees fairly well between observations and simulations. Also shown is the downwind variation of the column maximum radar reflectivity (Figure 5b), which is a measure of plume dilution and debris fall out. The maximum reflectivity (uncorrected) is ∼30 dbZ, with a logarithmic decay to the east. The sharpest reduction in reflectivity is close to the main updraft, suggesting the potential for ember fall out in this region.

6. Discussion and Conclusions

In this article, we present observations and numerical model simulations of the Marshall Fire in December 2021, which spread rapidly in the WUI due to strong, downslope winds along with dry, fine fuels and ember spotting. Such intense winds in this region occur nearly every year (NOAA Physical Sciences Laboratory, 2022), suggesting that the meteorological conditions were not uncommon. Measurements from surface stations and satellite show that the simulated fire propagates too slowly through wildland fuels at the beginning of the event, likely due to a general underestimation of the strongest wind speeds. Similar underestimation is also seen during Sundowner

events in wildfire-prone southern California (e.g., Cannon et al., 2017), highlighting modeling challenges related to complex topography.

For the first time, the complex three-dimensional atmospheric flow structure during the Marshall Fire is revealed through the DOW radar and turbulence-resolving WRF-Fire simulations. The radar retrievals illustrate substantial horizontal variability in the low-level wind field, in addition to vertical plume structure embedded in a robust hydraulic jump. WRF-Fire suggests that the highly variable, low-level winds are related to the hydraulic jump. In this jump region, the flow transitions from intense westerlies to much weaker westerlies or even a shift to easterlies, ultimately affecting the Marshall Fire spread rate and direction. It is likely that the small errors in the modeled microscale flow variability contribute to the differences in observed and modeled fire spread rate and direction as the fire approaches the towns of Superior and Louisville. Nonetheless, additional sources of model uncertainty (e.g., fuel moisture) should be more deeply examined in future fire studies to better understand the impact on fire spread and behavior.

Even though the model produces generally encouraging results, there are two main shortcomings related to the fire module in WRF that should be discussed. First, while the most up-to-date version of WRF-Fire as of this writing (version 4.4) contains a firebrand parameterization, it does not ignite spot fires, but rather provides only a likelihood of spot fire ignition. Rapid wildfire spread is often caused by embers generating new ignitions ahead of the main fire front (e.g., N. P. Lareau et al., 2022). The Marshall Fire was able to cross Highway-36, which is six-lanes wide. Such advancement is possible only through ember spotting. Therefore, a WRF-Fire simulation without additional manual ignitions, such as in this study, is not able to produce further fire spread.

Second, the WRF-Fire model must be improved to account for WUI fuels and related fire propagation in the built environment. During post-fire investigations of the Marshall Fire, the Institute for Business and Homes Safety found evidence that wooden fences falling between homes in Superior and Louisville were a primary cause of fire spread (Reppenhagen, 2022). At present, the WRF-Fire model contains fuel categories (based on Anderson 13) strictly intended for fires in the wildland and a rate of spread parameterization (based on Rothermel) developed using empirical laboratory fits to account for the effects of wind and slope. However, given the increasing trend in WUI fire occurrence, fuel maps including WUI materials, as well as improved representation of fire spread, should be developed for coupled fire-atmosphere models. As an additional step, more complex models (i.e., with full representation of combustion processes) combined with machine learning could be leveraged to improve fire spread parameterizations within coupled fire-atmosphere models. Lastly, we highlight that urban models (e.g., Masoudvaziri et al., 2021) are currently being used to help inform WUI fire spread, with emerging graphics processing unit-accelerated LES methods (e.g., Sauer & Muñoz-Esparza, 2020) becoming increasingly attractive platforms. The WUI challenge highlights the urgent need to better understand the complex interactions between humans and the built environment, weather, and wildfire, and ultimately develop more effective solutions to predict wildfire behavior and risk.

Data Availability Statement

Surface weather station data and model outputs (https://doi.org/10.7910/DVN/M6WCBT; T. Juliano et al., 2022) as well as VIIRS fire detection retrievals (https://doi.org/10.7910/DVN/PR6XDM; T. Juliano & Shamsaei, 2022) are stored on Harvard Dataverse. DOW measurements are available at (https://doi.org/10.48514/JKJ0-TE44; Wurman & Kosiba, 2023) through Zenodo. The WRF v4.4 code used for the simulations is publicly available on Github (https://github.com/wrf-model/WRF/tree/release-v4.4). Codes for the model (https://doi.org/10.7910/DVN/M6WCBT; T. Juliano et al., 2022) and DOW (https://doi.org/10.7910/DVN/KYSLUE; N. Lareau, 2022) analyses are available on Harvard Dataverse.

References

Abatzoglou, J. T., & Williams, A. P. (2016). Impact of anthropogenic climate change on wildfire across western US forests. *Proceedings of the National Academy of Sciences of the United States of America*, *113*(42), 11770–11775. https://doi.org/10.1073/pnas.1607171113

Balch, J. K., Bradley, B. A., Abatzoglou, J. T., Nagy, R. C., Fusco, E. J., & Mahood, A. L. (2017). Human expansion of the fire niche. *Proceedings of the National Academy of Sciences of the United States of America*, *114*(11), 2946–2951. https://doi.org/10.1073/pnas.1617394114

Ball, F. K. (1956). The theory of strong katabatic winds. *Australian Journal of Physics*, *9*(3), 373–386. https://doi.org/10.1071/ph560373

Brewer, M. J., & Clements, C. B. (2019). The 2018 Camp Fire: Meteorological analysis using in situ observations and numerical simulations. *Atmosphere*, *11*(1), 47. https://doi.org/10.3390/atmos11010047

Buchholz, R. R., Park, M., Worden, H. M., Tang, W., Edwards, D. P., Gaubert, B., et al. (2022). New seasonal pattern of pollution emerges from changing North American wildfires. *Nature Communications*, *13*(1), 2043. https://doi.org/10.1038/s41467-022-29623-8

Burke, M., Driscoll, A., Heft-Neal, S., Xue, J., Burney, J., & Wara, M. (2021). The changing risk and burden of wildfire in the United States. *Proceedings of the National Academy of Sciences of the United States of America*, *118*(2), e2011048118. https://doi.org/10.1073/pnas.2011048118

Bush, B., Anno, G., McCoy, R., Gaj, R., & Small, R. D. (1991). Fuel loads in US cities. *Fire Technology*, *27*(1), 5–32. https://doi.org/10.1007/bf01039525

Cannon, F., Carvalho, L. M., Jones, C., Hall, T., Gomberg, D., Dumas, J., & Jackson, M. (2017). WRF simulation of downslope wind events in coastal Santa Barbara County. *Atmospheric Research*, *191*, 57–73. https://doi.org/10.1016/j.atmosres.2017.03.010

Chanson, H. (2009). Current knowledge in hydraulic jumps and related phenomena: A survey of experimental results. *European Journal of Mechanics - B: Fluids*, *28*(2), 191–210. https://doi.org/10.1016/j.euromechflu.2008.06.004

Clark, T. L., Coen, J., & Latham, D. (2004). Description of a coupled atmosphere–fire model. *International Journal of Wildland Fire*, *13*(1), 49–63. https://doi.org/10.1071/wf03043

Coen, J. L. (2013). *A description of the coupled atmosphere-wildland fire environment model (CAWFE)* (Vol. 38). National Center for Atmospheric Research.

Coen, J. L., Cameron, M., Michalakes, J., Patton, E. G., Riggan, P. J., & Yedinak, K. M. (2013). WRF-Fire: Coupled weather–wildland fire modeling with the Weather Research and Forecasting model. *Journal of Applied Meteorology and Climatology*, *52*(1), 16–38. https://doi.org/10.1175/jamc-d-12-023.1

Coen, J. L., Schroeder, W., & Quayle, B. (2018). The generation and forecast of extreme winds during the origin and progression of the 2017 Tubbs Fire. *Atmosphere*, *9*(12), 462. https://doi.org/10.3390/atmos9120462

Cruz, M. G., Sullivan, A. L., Gould, J. S., Sims, N. C., Bannister, A. J., Hollis, J. J., & Hurley, R. J. (2012). Anatomy of a catastrophic wildfire: The black Saturday Kilmore east fire in Victoria, Australia. *Forest Ecology and Management*, *284*, 269–285. https://doi.org/10.1016/j.foreco.2012.02.035

DeCastro, A. L., Juliano, T. W., Kosović, B., Ebrahimian, H., & Balch, J. K. (2022). A computationally efficient method for updating fuel inputs for wildfire behavior models using Sentinel imagery and random forest classification. *Remote Sensing*, *14*(6), 1447. https://doi.org/10.3390/rs14061447

Dennison, P., Brewer, S., Arnold, J., & Moritz, M. (2014). Large wildfire trends in the western United States. *Geophysical Research Letters*, *41*(8), 2928–2933. https://doi.org/10.1002/2014gl059576

Durran, D. R. (1990). Mountain waves and downslope winds. In W. Blumen (Ed.), *Atmospheric processes over complex terrain, meteorological monographs* (Vol. 23, pp. 59–81). American Meteorological Society.

Efthimiou, N., Psomiadis, E., & Panagos, P. (2020). Fire severity and soil erosion susceptibility mapping using multi-temporal Earth Observation data: The case of Mati fatal wildfire in Eastern Attica. *Catena*, *187*, 104320. https://doi.org/10.1016/j.catena.2019.104320

Fovell, R. G., Brewer, M. J., & Garmong, R. J. (2022). The December 2021 Marshall Fire: Predictability and gust forecasts from operational models. *Atmosphere*, *13*(5), 765. https://doi.org/10.3390/atmos13050765

Fovell, R. G., & Gallagher, A. (2018). Winds and gusts during the Thomas fire. *Fire*, *1*(3), 47. https://doi.org/10.3390/fire1030047

Ganteaume, A. (2020). Role of ornamental vegetation in the propagation of the Rognac Fire. In S. M. Hood, S. Drury, T. Steelman, & R. Steffens (Eds.), *Proceedings of the fire continuum-preparing for the future of wildland fire*, *Research station: A special report of working groups I and II of the intergovernmental panel on climate change (IPCC)* (pp. 25–64). US Department of Agriculture, Forest Service, Cambridge University Press.

Haupt, S. E., Kosović, B., Shaw, W., Berg, L. K., Churchfield, M., Cline, J., et al. (2019). On bridging a modeling scale gap: Mesoscale to microscale coupling for wind energy. *Bulletin America Meteorology Social*, *1009*(12), 2533–2550. https://doi.org/10.1175/bams-d-18-0033.1

Iglesias, V., Balch, J., & Travis, W. R. (2022). U.S. fires became larger, more frequent, and more widespread in the 2000s. *Science Advances*, *8*(11). https://doi.org/10.1126/sciadv.abc0020

Juliano, T., Frediani, M., Shamsaei, K., Eghdami, M., & Kosovic, B. (2022). WRF-fire files for "toward a better understanding of wildfire behavior in the wildland-urban interface: A case study of the 2021 Marshall Fire". *Harvard Dataverse, V5*. https://doi.org/10.7910/DVN/M6WCBT

Juliano, T., & Shamsaei, K. (2022). VIIRS files for "toward a better understanding of wildfire behavior in the wildland-urban interface: A case study of the 2021 Marshall fire". *Harvard Dataverse, V1*. https://doi.org/10.7910/DVN/PR6XDM

Juliano, T. W., Jiménez, P. A., Kosović, B., Eidhammer, T., Thompson, G., Berg, L. K., et al. (2022). Smoke from 2020 United States wildfires responsible for substantial solar energy forecast errors. *Environmental Research Letters*, *17*(3), 034010. https://doi.org/10.1088/1748-9326/ac5143

Juliano, T. W., Parish, T. R., Rahn, D. A., & Leon, D. C. (2017). An atmospheric hydraulic jump in the Santa Barbara Channel. *Journal of Applied Meteorology and Climatology*, *56*(11), 2981–2998. https://doi.org/10.1175/jamc-d-16-0396.1

Keeley, J. E., & Syphard, A. D. (2019). Twenty-first century California, USA, wildfires: Fuel-dominated vs. wind-dominated fires. *Fire Ecology*, *15*(1), 24. https://doi.org/10.1186/s42408-019-0041-0

Lareau, N. (2022). DOW files for "toward a better understanding of wildfire behavior in the wildland-urban interface: A case study of the 2021 Marshall fire". *Harvard Dataverse, V2*. https://doi.org/10.7910/DVN/KYSLUE

Lareau, N. P., Donohoe, A., Roberts, M., & Ebrahimian, H. (2022). Tracking wildfires with weather radars. *Journal of Geophysical Research: Atmospheres*, *127*(11), e2021JD036158. https://doi.org/10.1029/2021jd036158

Lawson, J., & Horel, J. (2015). Ensemble forecast uncertainty of the 1 December 2011 Wasatch downslope windstorm. *Weather and Forecasting*, *30*(6), 1749–1761. https://doi.org/10.1175/waf-d-15-0034.1

Liu, Y. C., Di, P., Chen, S. H., Chen, X., Fan, J., DaMassa, J., & Avise, J. (2021). Climatology of Diablo winds in northern California and their relationships with large-scale climate variabilities. *Climate Dynamics*, *56*(3–4), 1335–1356. https://doi.org/10.1007/s00382-020-05535-5

Masoudvaziri, N., Bardales, F. S., Keskin, O. K., Sarreshtehdari, A., Sun, K., & Elhami-Khorasani, N. (2021). *Streamlined wildland-urban interface fire tracing (SWUIFT): Modeling wildfire spread in communities* (Vol. 143). Environmental Modelling & Software.

Mass, C. F., & Ovens, D. (2019). The Northern California wildfires of 8–9 October 2017: The role of a major downslope wind event. *Bulletin America Meteorology Social*, *100*(2), 235–256. https://doi.org/10.1175/bams-d-18-0037.1

Mass, C. F., & Ovens, D. (2021). The synoptic and mesoscale evolution accompanying the 2018 Camp Fire of Northern California. *Bulletin America Meteorology Social*, *102*(1), E168–E192. https://doi.org/10.1175/bams-d-20-0124.1

Mazzaro, L. J., Muñoz-Esparza, D., Lundquist, J. K., & Linn, R. R. (2017). Nested mesoscale-to-LES modeling of the atmospheric boundary layer in the presence of under-resolved convective structures. *Journal of Advances in Modeling Earth Systems*, *9*(4), 1795–1810. https://doi.org/10.1002/2017ms000912

Muñoz-Esparza, D., Lundquist, J. K., Sauer, J. A., Kosović, B., & Linn, R. R. (2017). Coupled mesoscale-LES modeling of a diurnal cycle during the CWEX-13 field campaign: From weather to boundary-layer eddies. *Journal of Advances in Modeling Earth Systems*, *9*(3), 1572–1594. https://doi.org/10.1002/2017ms000960

Nauslar, N. J., Abatzoglou, J. T., & Marsh, P. T. (2018). The 2017 north Bay and southern California fires: A case study. *Fire*, *1*(18), 18. https://doi.org/10.3390/fire1010018

NOAA Physical Sciences Laboratory. (2022). Boulder wind info. Retrieved from https://psl.noaa.gov/boulder/wind.html

Radeloff, V. C., Helmers, D. P., Kramer, H. A., Mockrin, M. H., Alexandre, P. M., Bar-Massada, A., et al. (2018). Rapid growth of the US wildland-urban interface raises wildfire risk. *Proceedings of the National Academy of Sciences of the United States of America*, *115*(13), 3314–3319. https://doi.org/10.1073/pnas.1718850115

Rai, R. K., Berg, L. K., Kosović, B., Haupt, S. E., Mirocha, J. D., Ennis, B., & Draxl, C. (2019). Evaluation of the impact of horizontal grid spacing in terra incognita on coupled mesoscale-microscale simulations using the WRF framework. *Monthly Weather Review*, *147*(3), 1007–1027. https://doi.org/10.1175/mwr-d-18-0282.1

Raphael, M. N. (2003). The Santa Ana winds of California. *Earth Interactions*, *7*(8), 1–13. https://doi.org/10.1175/1087-3562(2003)007<0001:tsawoc>2.0.co;2

Reppenhagen, C. (2022). *Wood fences found to be pathways for Marshall Fire to spread between homes*. 9NEWS. Retrieved from https://www.9news.com/article/news/local/wildfire/marshall-fire/wood-fences-pathways-for-marshall-fire-spread/73-7ba1eafc-196a-48c9-abfe-46f87189b2b4

Sauer, J. A., & Muñoz-Esparza, D. (2020). The FastEddy™ resident-GPU accelerated large-eddy simulation framework: Model formulation, dynamical-core validation and performance benchmarks. *Journal of Advances in Modeling Earth Systems*, *12*, e2020MS002100. https://doi.org/10.1029/2020MS002100

Shamsaei, K., Juliano, T. W., Roberts, M., Ebrahimian, H., Kosović, B., Lareau, N. P., & Taciroglu, E. (2023). Coupled fire-atmosphere simulation of the 2018 Camp Fire using WRF-Fire. *International Journal of Wildland Fire*, *32*(2), 195–221. https://doi.org/10.1071/wf22013

Skamarock, W. C., Klemp, J. B., Dudhia, J., Gill, D. O., Liu, Z., Berner, J., et al. (2019). A description of the advanced Research WRF version 4. NCAR Tech. Note NCAR/TN-556+STR.

Smith, C., Hatchett, B. J., & Kaplan, M. (2018). A surface observation based climatology of diablo-like winds in California's wine country and western Sierra Nevada. *Fire*, *1*(25), 25. https://doi.org/10.3390/fire1020025

Westerling, A. L., Hidalgo, H. G., Cayan, D. R., & Swetnam, T. W. (2006). Warming and earlier spring increase western U.S. forest wildfire activity. *Science*, *313*(5789), 940–943. https://doi.org/10.1126/science.1128834

Whiteman, D. C., & Whiteman, J. G. (1974). An historical climatology of damaging downslope windstorms at Boulder, Colorado. NOAA technical report ERL; 336; NOAA technical report ERL. 35 APCL.

Wurman, J., & Kosiba, K. (2023). Flexible Array of Radars and Mesonets Marshal Fire (2021) data (Version 1) [Dataset]. https://doi.org/10.48514/JKJ0-TE44

Wurman, J., Kosiba, K., Pereira, B., Robinson, P., Frambach, A., Gilliland, A., et al. (2021). The FARM (Flexible Array of Radars and Mesonets). *Bulletin America Meteorology Social*, *102*, E1499–E1525. https://doi.org/10.1175/bams-d-20-0285.1

Wurman, J., Straka, J., Rasmussen, E., Randall, M., & Zahrai, A. (1997). Design and deployment of a portable, pencil-beam, pulsed, 3-cm Doppler radar. *Journal of Atmospheric and Oceanic Technology*, *14*(6), 1502–1512. https://doi.org/10.1175/1520-0426(1997)014<1502:dadoap>2.0.co;2

Yoon, J., Wang, S.-Y. S., Gillies, R. R., Hipps, L., Kravitz, B., & Rasch, P. J. (2015). Extreme fire season in California: A glimpse into the future? *Bulletin America Meteorology Social*, *96*(12), S5–S9. https://doi.org/10.1175/bams-d-15-00114.1

Yue, X., Mickley, L. J., Logan, J. A., & Kaplan, J. O. (2013). Ensemble projections of wildfire activity and carbonaceous aerosol concentrations over the western United States in the mid-21st century. *Atmospheric Environment*, *77*, 767–780. https://doi.org/10.1016/j.atmosenv.2013.06.003

References From the Supporting Information

Albini, F. A., & Reinhardt, E. D. (1995). Modeling ignition and burning rate of large woody natural fuels. *International Journal of Wildland Fire*, *5*(2), 81–91. https://doi.org/10.1071/wf9950081

Anderson, H. E. (1981). *Aids to determining fuel models for estimating fire behavior* (Vol. 122). US Department of Agriculture, Forest Service, Intermountain Forest and Range Experiment Station.

Benjamin, S. G., Weygandt, S. S., Brown, J. M., Hu, M., Alexander, C. R., Smirnova, T. G., et al. (2016). A North American hourly assimilation and model forecast cycle: The rapid refresh. *Monthly Weather Review*, *144*(4), 1669–1694. https://doi.org/10.1175/mwr-d-15-0242.1

Deardorff, J. W. (1980). Stratocumulus-capped mixed layers derived from a three-dimensional model. *Boundary-Layer Meteorology*, *18*(4), 495–527. https://doi.org/10.1007/bf00119502

Dudhia, J. (1989). Numerical study of convection observed during the winter monsoon experiment using a mesoscale two-dimensional model. *Journal of the Atmospheric Sciences*, *46*(20), 3077–3107. https://doi.org/10.1175/1520-0469(1989)046<3077:nsocod>2.0.co;2

Ek, M. B., Mitchell, K. E., Lin, Y., Rogers, E., Grunmann, P., Koren, V., et al. (2003). Implementation of Noah land surface model advances in the national centers for environmental prediction operational mesoscale Eta model. *Journal of Geophysical Research*, *108*(D22), 8851. https://doi.org/10.1029/2002jd003296

Frediani, M., Juliano, T. W., DeCastro, A., Kosović, B., & Knievel, J. (2021). A fire-spotting parameterization coupled with the WRF-fire model. *Earth and Space Science Open Archive*, *12*. https://doi.org/10.1002/essoar.10506771.1

Hong, S.-Y., Noh, Y., & Dudhia, J. (2006). A new vertical diffusion package with an explicit treatment of entrainment processes. *Monthly Weather Review*, *134*(9), 2318–2341. https://doi.org/10.1175/mwr3199.1

Horel, J., Splitt, M., Dunn, L., Pechmann, J., White, B., Ciliberti, C., et al. (2002). Mesowest: Cooperative Mesonets in the western United States. *Bulletin America Meteorology Social*, *83*(2), 211–226. https://doi.org/10.1175/1520-0477(2002)083<0211:mcmitw>2.3.co;2

Iacono, M. J., Delamere, J. S., Mlawer, E. J., Shephard, M. W., Clough, S. A., & Collins, W. D. (2008). Radiative forcing by long-lived greenhouse gases: Calculations with the AER radiative transfer models. *Journal of Geophysical Research*, *113*, D13103. https://doi.org/10.1029/2008jd009944

Jiménez, P. A., Dudhia, J., Gonzalez-Rouco, J. F., Navarro, J., Montavez, J. P., & Garcia–Bustamante, E. (2012). A revised scheme for the WRF surface layer formulation. *Monthly Weather Review*, *140*(3), 898–918. https://doi.org/10.1175/mwr-d-11-00056.1

Juliano, T. W., Kosović, B., Jiménez, P. A., Eghdami, M., Haupt, S. E., & Martilli, A. (2022). Gray Zone" simulations using a three-dimensional planetary boundary layer parameterization in the Weather Research and Forecasting model. *Monthly Weather Review*, *150*(7), 1585–1619. https://doi.org/10.1175/mwr-d-21-0164.1

Muñoz Esparza, D., Kosović, B., Jiménez, P. A., & Coen, J. L. (2018). An accurate fire-spread algorithm in the Weather Research and Forecasting model using the level-set method. *Journal of Advances in Modeling Earth Systems*, *10*(4), 908–926. https://doi.org/10.1002/2017ms001108

Rollins, M. G. (2009). LANDFIRE: A nationally consistent vegetation, wildland fire, and fuel assessment. *International Journal of Wildland Fire*, *18*(3), 235–249. https://doi.org/10.1071/wf08088

Rothermel, R. C. (1972). *A mathematical model for predicting fire spread in wildland fuels* (Vol. 115). USDA Forest Service Research Paper INT.

Schmidli, J. (2013). Daytime heat transfer processes over mountainous terrain. *Journal of the Atmospheric Sciences*, *70*(12), 4041–4066. https://doi.org/10.1175/jas-d-13-083.1

Smagorinsky, J. (1963). General circulation experiments with the primitive equations: I. The basic experiment. *Monthly Weather Review*, *91*(3), 99–164. https://doi.org/10.1175/1520-0493(1963)091<0099:gcewtp>2.3.co;2

Vaughan, K. (2022). *Videos show Marshall Fire started by 2 separate ignition points less than a mile apart*. 9NEWS. Retrieved from https://www.9news.com/article/news/local/wildfire/marshall-fire/marshall-fire-2-ignition-points/73-d3755c1c-120a-49cb-8ee0-ad0f1f1fc41a

Wagner, J. S., Gohm, A., & Rotach, M. W. (2014). The impact of horizontal model grid resolution on the boundary layer structure over an idealized valley. *Monthly Weather Review*, *142*(9), 3446–3465. https://doi.org/10.1175/mwr-d-14-00002.1